NUMERICAL METHOD FOR PRE-ARCING TIMES: APPLICATION IN HBC FUSES WITH HEAVY FAULT-CURRENTS

S. Memiaghe, W. Bussière and D. Rochette

LAEPT, 24 av des Landais, 63177 Aubiere Cedex France, E-mail :steeve.memiaghe@univ-bpclermont.fr

Abstract: **This works deals with calculations of pre-arcing time prediction for fuse links used in industrial protection circuits in case of heavy faults-currents. An enthalpy method to solve heat-transfer equation included two phase-changes is presented. The mathematical model couples thermal and electrical equations based on the principle of energy conservation and the Ohm's law respectively. In order to determine current density and temperature evolution in the fuses, three typical fuse links have been chosen for the calculations with circular, rectangular and trapezoidal reduced sections at their centre. Silver physical properties, mathematical equations and the numerical method are reported. Calculations results show that for the fuse link with rectangular reduced section a major heat-transfer mechanism took place compared to the other ones.**

Keywords: **High Breaking Capacity fuses, pre-arcing time, heavy fault-currents, Stefan problem, simulation.**

1. Introduction

The fuses studied which common name is High Breaking Capacities fuses comprise four main elements: a fuse link (usually silver of high purity) with one or series reduced sections named notches in different checked shapes, the filling cavity (mechanically and thermally resistant), and the filling silica sand (or quartz) of high purity. HBC fuses operate in two stages, pre-arcing operation and arcing operation. The pre-arcing operation corresponds to the time from the apparition of a high fault current to the vaporization of the constricted sections and the disruption of the fuse link.

The modelling of the pre-arcing stage has been the object of several works until now. These theoretical works consist in semi-empirical modelling or physical modelling dedicated to the pre-arcing stage [1, 2]. The theoretical works dedicated to the pre-arcing stages proposed various models based on the heat transfer occurring into different fuses design [3-6]. In these models the end of pre-arcing operation is defined by the time to reach the melting temperature of the fuse element. Thus for pre-arcing time prediction calculations are

lead until melting temperature is reached. In this paper a model which considers the phase-changes to describe heat-transfer occurring in the fuse is presented. The model is based on the solution of the heat-transfer equation via an enthalpy formulation which allows taking into account two phase-change problems. This method also called *Stefan problem*, has been studied in [7] and it is useful in other thermal problems involving phase changes [8, 9]. Calculations are performed for three fuse elements with different reduced sections shapes located at their centre .In the case of short prearcing time (up to 10 ms), where the fuse-element temperature rising is almost adiabatic [8], a high overload current is applied, heat-loss is governed only by thermal conduction and other heat-loss mechanism are neglected. The heat-transfer equation is a mathematical equation coupling thermal and electrical equations.

We present in a first time, fuse-links geometries and physicals properties of silver, following by the modelling equations, which stand for thermal and electrical phenomena, the imposed hypotheses of the model and the numerical procedure, are developed in section 3. In section 4 we show and discuss the numerical results.

2. Geometrical hypotheses and physical data

2.1. Fuse links description

The fuse links studied have circular, rectangular and trapezoidal reduced sections located at their centre.

The geometries of the three tested fuse elements are presented in figure 1. The fuse links have cross section and reduced section of respectively *le= 2.5×0.105 mm²* and *l'e=0.5×0.105 mm²*, where *e* is the thickness of the fuse link. The fuse links lengths are *L=70 mm* and are made from pure silver strip (99.95%). The following areas are defined for the numerical treatment:

Ω fuse-element area, Γ_1 *anode*,

Γ_2 cathode, $\Gamma_{3,4}$ *fuse−boundaries*
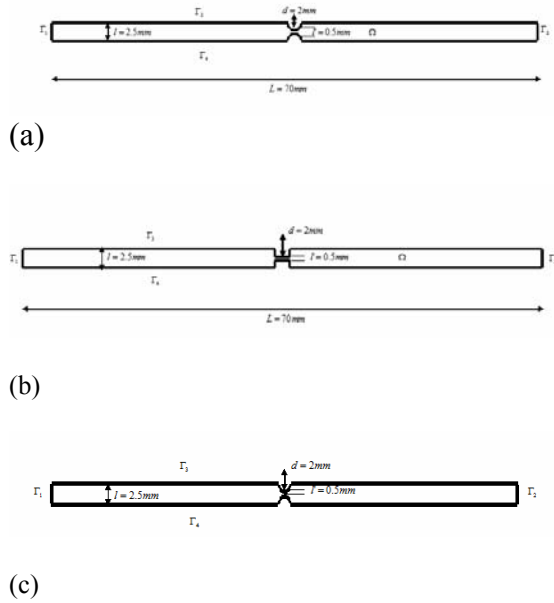
(a)

(b)

(c)

Fig. 1: 2-D geometries of the fuse links.

2.2. Physical properties of Silver

Table 1 presents thermodynamical data use in the computations; the parameters depending on temperature are given at reference temperature. The evolutions of the physical properties as functions of the temperature are in the following figures.

Table 1: Physical properties of the Silver

Silver density	$\rho = 10500\ kg.m^{-3}$ at 293 K
Thermal conductivity	$k = 452\ W.m^{-1}.K^{-1}$ at 293 K
Electrical conductivity	$\sigma = 64.17 \times 10^6\ S.m^{-1}$ at 293 K
Solid heat capacity	$c_s = 261.36\ J.kg^{-1}.K^{-1}$ at 293 K
Liquid heat capacity	$c_l = 310.4\ J.kg^{-1}.K^{-1}$ at 1235 K
Melting temperature	$T_m = 1235\ K$
Boiling temperature	$T_v = 2433\ K$
Melting latent heat	$L_f = 1.05 \times 10^5\ J.kg^{-1}$
Vaporization latent heat	$L_{vap} = 2.43 \times 10^6\ J.kg^{-1}$

The most used and complete thermal conductivities for silver are quoted in *Touloukian* tables [10]. Figure 2 presents silver thermal conductivity as a function of temperature for silver. It can be seen a strong decrease of thermal conductivity during the

solid to liquid phase-change. This thermal conductivity de-crease is of :
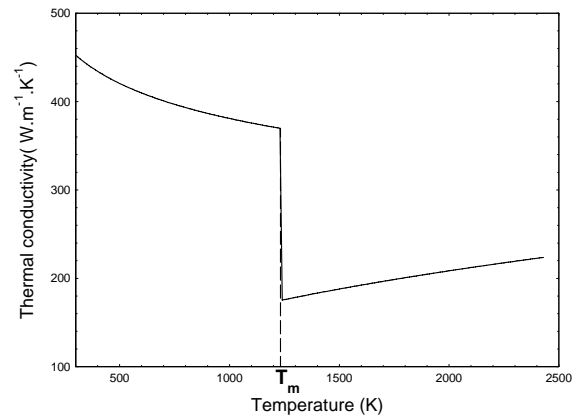$$k_s(T_m) - k_l(T_m) = 177.92\ W.m^{-1}.K^{-1}.$$

Fig. 2: Thermal conductivity versus temperature.

Figure 3 shows two type of data concerning electrical conductivity which occurs in the Joule heating term. The electrical conductivity has been measured (continuous lines) [11] and calculated (dashed lines) by means of *Wiedemann and Franz* law [12] which is written in terms of:

$$\frac{k}{\sigma} = L \times T, \qquad (1)$$

where $L = 2.45 \times 10^8 V^2 K^2$ is the *Lorenz* coefficient, T is the temperature, k and σ are respectively the thermal and the electrical conductivity.
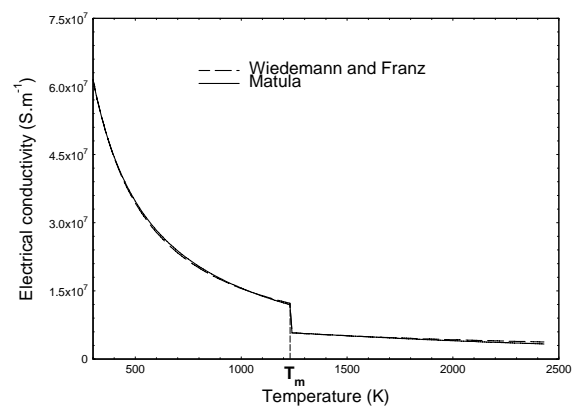

Fig. 2: Electrical conductivities versus temperature measured (dashed lines) calculated (continuous lines).

As electrical conductivity is concerned, it can be seen from the figure that an electrical conductivity

decreases of $\sigma_s(T_m) - \sigma_l(T_m) = 6.1037 \times 10^6$ S.m^{-1} when phase-change occurs.

A very good agreement is observed between the measured and the calculated values.

Figure 4 shows the enthalpy as a function of temperature. It can be seen from the figure two jumps named melting latent heat L_f and vaporisation latent heat L_v. This figure is an enthalpy formulation of the Stefan problem.
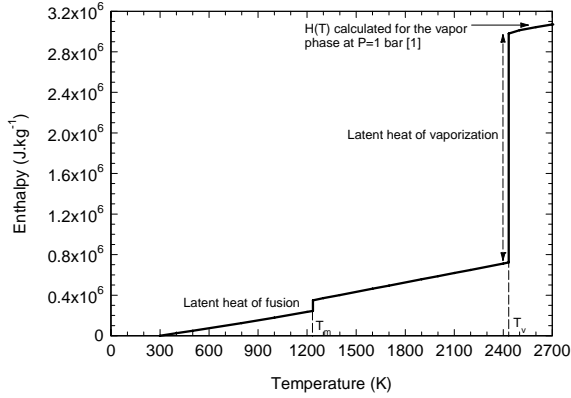

Fig. 3 : Enthalpy versus temperature [13].

3. Physical model of the fuse element heating and numerical method

Heat transfer equation is obtained by expressing heat balance equation, based on principle of energy conservation, expressing a balance between heat-loss mechanism and power injected:

$$\frac{\partial H}{\partial t} - \mathbf{div}.(k\mathbf{grad}T) = S, \qquad (2)$$

Where H is the volumetric enthalpy, k is the thermal conductivity, T is the temperature. The source term representing the heat generated by Joule heating writes:

$$S = \frac{|\mathbf{J}|^2}{\sigma}, \qquad (3)$$

where $\mathbf{J}$ is the current density vector and σ is the electrical conductivity.

To solve numerically the heat equation, a reciprocal form of $H(T)$ is defined as $\beta(H(T)) = T$ [7], and the Stefan problem in enthalpy-temperature, with boundaries and initial conditions is given by the set of equations:

$$\begin{cases} \dfrac{\partial H}{\partial t} - \mathbf{div}.(k\mathbf{grad}T) = \dfrac{|\mathbf{J}|^2}{\sigma}, & \text{in } \Omega \times [0,t] \\ T = \beta(T), & \text{in } \Omega \times [0,t] \\ k(T)\dfrac{\partial T}{\partial \mathbf{n}} = 0, & \text{on } \Gamma_{1,2,3,4} \times [0,t] \\ H = H_0, & \text{in } \Omega, \text{ for } t = 0 \end{cases} \qquad (4)$$

where H_0 is an initial condition stands for enthalpy at time $t=0$. The Joule heating in equation (3) is obtained by solving the following equations:

$$\begin{cases} \mathbf{div}.(\sigma\mathbf{grad}\,V) = 0, & \text{in } \Omega \\ \sigma(T)\dfrac{\partial V}{\partial \mathbf{n}} = \dfrac{I(t)}{|\Gamma_1|}, & \text{on } \Gamma_1 \times [0,t] \\ \sigma(T)\dfrac{\partial V}{\partial \mathbf{n}} = 0, & \text{on } \Gamma_{3,4} \\ V = 0, & \text{on } \Gamma_2 \\ \mathbf{E} = -\mathbf{grad}\,V, & \text{in } \Omega \\ \mathbf{J} = \sigma\mathbf{E}, & \text{in } \Omega \end{cases} \qquad (5)$$

where V, $\mathbf{E}$ and $I(t)$ are respectively the electric potential, the electric field vector and the electric current. $\mathbf{n}$ is the outward unit normal to the boundary. We have prescribed the following boundary conditions:

- on Γ_1 defined as the anode, a Neumann condition is imposed for the current density flux;
- a Dirichlet condition for the potential in Γ_2 defined as the cathode;
- for the other boundaries a homogeneous Neumann condition is assumed.

To solve numerically the thermal electric problem (equations (4) and (5)), we use in the space discretization a standard finite element method [14], and the time integration of the heat equation (4) is performed by using a Chernoff scheme [7] which consists in the relaxation of the relation $H(T)$ (Figure 4).

4. Numerical results

Numerical results are given for the temperature, the Joule heating, the potential and the resistance evolutions for the three tested fuse links. For the evaluation of the pre-arcing time in fuse-links the calculations are led with the prospective current given by Equation (6) until the vaporization enthalpy is reached. For each fuse element the following voltage characteristics are used to remain in the short pre-arcing time domain: a maximum voltage of $\hat{V} = 300\sqrt{2}$ V.

The prospective current use in calculations is written as:

$$I(t) = \frac{\hat{V}}{\sqrt{R^2 + L^2\omega^2}} \times \left(\sin(\omega t + \theta - \varphi) - \sin(\theta - \varphi) \times e^{-\frac{R}{L}t} \right)$$

(6)

where $\hat{V}$ is the supplied voltage, R is the resistive load, L is the inductive load, ω is the pulsation at 50 Hz, θ is the closing angle, $\cos\varphi$ is the power factor, t is the time.

The figure 5 shows examples of a non-structured 2-D meshes uses in calculations for the three tested fuse links, the mesh being performed using the mesh generator software *GMSH* [15]. The fuse elements meshes are composed of *7308* triangle cells and *3655* nodes for the circular notch (a), 7148 triangle cells and 3575 nodes for the rectangular notch (b) and of 7446 triangle cells and 3724 nodes for the trapezoidal notch (c); the reduced sections are meshed as more finely.
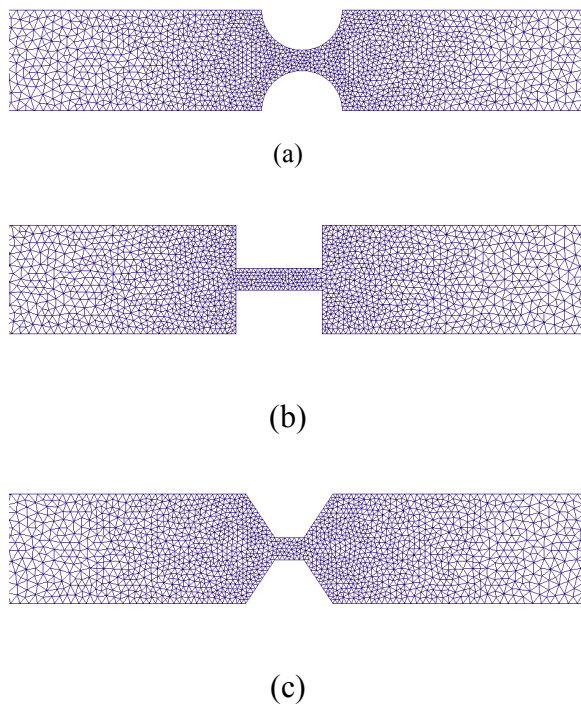

(a)

(b)

(c)

Fig. 4: Fuse links meshes.

Temperature at the initial time is fixed at $T_0=300K$, the time step is fixed at $\Delta t=10^{-5}s$ and calculations are stopped once the enthalpy of vaporization is reached.
Figure 6 illustrates an example of 2-D cartography of the temperature distribution in the fuse links at the end of pre-arcing time obtained at *t=3.9 ms* for the three fuse links.
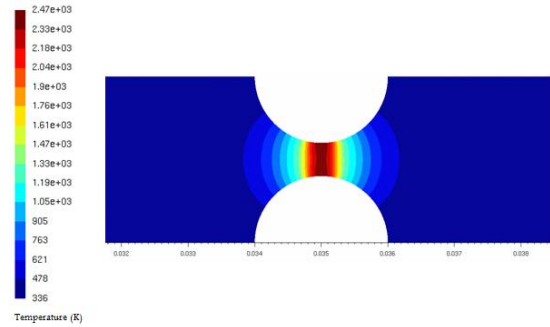

Fig. 5: Isothermal distributions in the fuse-element at the end of prearcing time.

It can be seeing that the temperature rise takes place in the notch centre where isothermal contours are induced by the reduced sections shape. This is clearly demonstrated in figure 7 which presents temperature distribution along the fuse for the three reduced sections fuse links just before the creation of electric arc. The peak of temperature stand for the rectangular notch fuse link has a width of around 2 times the circular and the trapezoidal ones.
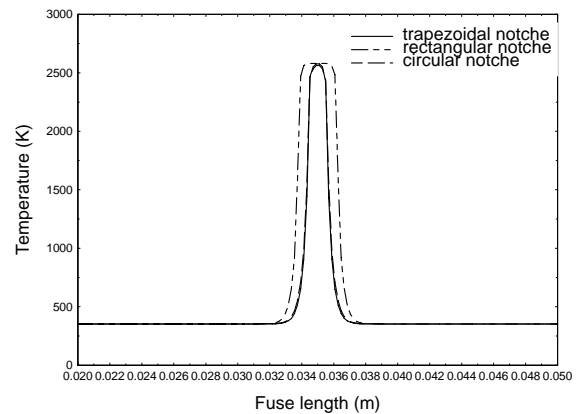

Fig. 6: Temperature distribution in the fuse-link following the x-direction at *y=1.25mm*.

Figure 8 presents the temperature history during the pre-arcing time for the three considered fuse links. The temperature of the fuse links evolve according to four stages: a gradual increase up to the melting temperature, followed by the phase change at constant temperature during a lapse time. The third stage which corresponds to the strong temperature rise due to the high resistivity of the fuse links and the last stage corresponds to liquid vapour transition. The time necessary to this transition is longer due to the latent heat of vaporization which is about 20 times the latent heat of fusion as previously given in Table 1.
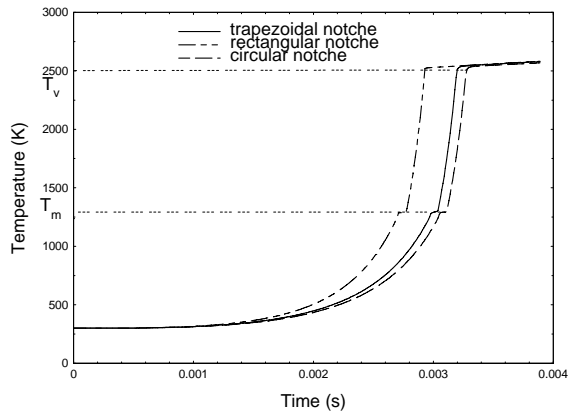
Fig 7: Temperature history at positions *x =35 mm* for *y = 1.25 mm* for the three fuse links.

It is noteworthy to note that for the rectangular notch fuse link, the temperature rise up to the vaporization temperature is faster than the two others fuse links and the liquid vapour transition time is longer than the other ones. Indeed due to the abrupt constricted section at the centre of the rectangular notch fuse link, a fast and strong increase of Joule effect induced by a maximum of current density is observed in figure 9.

The joule heating history versus time has the four stages previously quoted. Concerning the last stage a joule heating increase is observed due only to the current density rise. Indeed the electrical resistivity is almost constant after the vaporization temperature.
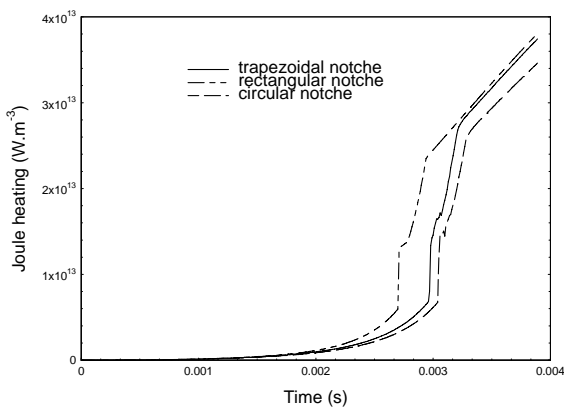

Fig. 8: Joule heating rise of the three fuse links during the pre-arcing time, at positions *x =35 mm* for *y = 1.25 mm.*

Figure 10a and figure 10b presents respectively the calculated evolutions of resistance and voltage of the three fuse links as functions of time.
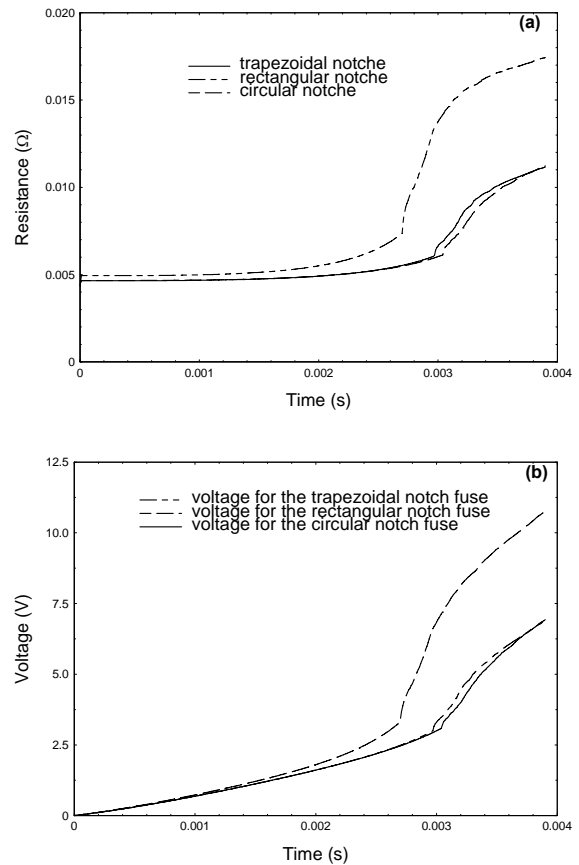

Fig. 9: Voltage and resistance histories versus time for three fuse links.

The voltage curves and the resistance curves show a two-step evolution: the first step is characterized by a slow increase and the second step is characterized by a fast increase. This is due to the silver resistivity which is 2 times more important in the liquid state than in the solid state and consequently the voltage evolution has same characteristics.

5. Conclusion

A model to predict pre-arcing time in heavy fault currents applied to HBC fuses has been presented. The model is based on the solution of heat-transfer equation including two phase-changes. Thermal conduction and Joule heating are respectively, the major heat-loss and heat source. The enthalpy method is used of calculating short pre-arcing times in three silver typical fuse links. A comparison between the numerical results shows that for the fuse link with rectangular notch a fast and strong Joule heating due to a highest resistivity than the two others. A maximum of energy correspond to the latent heat of vaporization is necessary to

vaporize and to allow the disruption of the fuse links.

Acknowledgments

References

[1] J.G. Leach, P.G. Newbery, A. Wright, "Analysis of high-rupturing-capacity fuse-link prearcing phenomena by a finite-difference method", Proceedings of the IEE, vol. 120, n°9, September, 987-993 (1973).

[2] L.A.V. Cheim, A.F. Howe, "Calculating fuse pre-arcing times by transmission-line modelling (TLM)", Proceedings of the 4th International Conference on Electric Fuses and their Applications, Nottingham, 162-167 (1991).

[3] M. S. Agarwal, A D Stokes and P Kovitya, "Pre-arcing behaviour of open fuse wire", J. Phys. D: Appl. Phys 20, 1237-1242 (1987).

[4] M. Sasu and G. Oarga, "Simulation of the heat transfer phenomena in variable section fusible elements in non-adiabatic regime", Archiv für Elektrotechnik, 75, 425-431 (1992).

[5] C. Garrido and J. Cidras, "A method for predicting time-current characteristics of fuselinks", Electric Machines and Power Systems, 26, 685-698 (1998).

[6] Y. Kawase, T. Miyatake, and S. Ito, "Heat Analysis of a Fuse for Semiconductor Devices Protection Using 3-D Finite Element Method", IEEE TRANSACTIONS ON MAGNETICS, vol. 36, no.4 (July 2000).

[7] G. Amiez, P.A. Gremeau, "On a numerical approach to Stefan-like problems". Numerische Mathematik, 59, 71-89 (1991).

[8] D. Rochette, R. Touzani, W. Bussiere, "Numerical study of the short pre-arcing time in HBC fuses via an enthalpy formulation", J. Phys. D: Appl. Phys 40 (2007) 4544-4551.

[9] Y. Safa, "Simulation numérique des phénomènes thermiques et magnétohydrodynamiques dans une cellule de Hall-Héroult", Thèse EPFL no 3185 (2005).

[10] Y.S.Touloukian, R.W. Powell and C.Y. Ho, "Thermal conductivity - metallic elements and alloys", Vol. 1 of Thermophysical properties of Matter – the TPRC Data Series, ed. IFI/Plenum New York Washington (1970).

[11] R.A. Matula, "Electrical Resistivity of Copper, Gold, Palladium, and Silver", JPCRD 8(4), 1147-1298 (1979).

[12] J.L. Bretonnet, "Conductivité électrique des métaux liquides", Techniques de l'ingénieur MB2 (2005).

[13] I. Bahrin, "Thermochemical Data of Pure Substances", 3rd ed. in collaboration with G. Platzki, vol. 1. Ag-Kr and vol. 2. La-Zr, VCH Weinheim, Federal Republic of Germany, New York (1995).

[14] J-M. Bergheau, "Simulation numérique des transferts thermiques par éléments finis", © LAVOISIER (2004).

[15] C. Geuzaine and J.F. Remacle, GMSH, http://www.geuz.org/gmsh/.